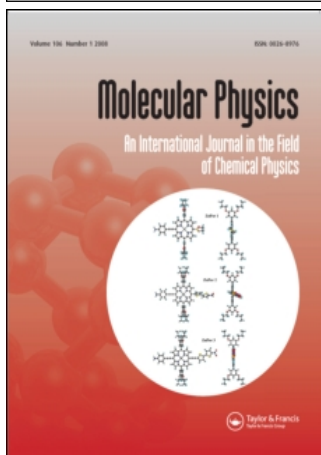


This article was downloaded by:[Max Planck Inst & Research Groups Consortium]  
On: 23 April 2008  
Access Details: [subscription number 789998295]  
Publisher: Taylor & Francis  
Informa Ltd Registered in England and Wales Registered Number: 1072954  
Registered office: Mortimer House, 37-41 Mortimer Street, London W1T 3JH, UK



## Molecular Physics

### An International Journal in the Field of Chemical Physics

Publication details, including instructions for authors and subscription information:  
<http://www.informaworld.com/smpp/title~content=t713395160>

#### Strong-field control of electron localisation during molecular dissociation

M. F. Kling<sup>ab</sup>, Ch. Siedschlag<sup>a</sup>, I. Znakovskaya<sup>b</sup>, A. J. Verhoef<sup>b</sup>, S. Zherebtsov<sup>b</sup>, F. Krausz<sup>bc</sup>, M. Lezius<sup>b</sup>, M. J. J. Vrakking<sup>a</sup>

<sup>a</sup> FOM Instituut voor Atoom en Moleculair Fysica (AMOLF), Amsterdam, 1098 SJ, The Netherlands

<sup>b</sup> Max-Planck-Institut für Quantenoptik, D-85748 Garching, Germany

<sup>c</sup> Department für Physik, Ludwig-Maximilians-Universität München, D-85748 Garching, Germany

Online Publication Date: 01 January 2008

To cite this Article: Kling, M. F., Siedschlag, Ch., Znakovskaya, I., Verhoef, A. J., Zherebtsov, S., Krausz, F., Lezius, M. and Vrakking, M. J. J. (2008) 'Strong-field control of electron localisation during molecular dissociation', Molecular Physics, 106:2, 455 - 465

To link to this article: DOI: 10.1080/00268970701864739

URL: <http://dx.doi.org/10.1080/00268970701864739>

PLEASE SCROLL DOWN FOR ARTICLE

Full terms and conditions of use: <http://www.informaworld.com/terms-and-conditions-of-access.pdf>

This article maybe used for research, teaching and private study purposes. Any substantial or systematic reproduction, re-distribution, re-selling, loan or sub-licensing, systematic supply or distribution in any form to anyone is expressly forbidden.

The publisher does not give any warranty express or implied or make any representation that the contents will be complete or accurate or up to date. The accuracy of any instructions, formulae and drug doses should be independently verified with primary sources. The publisher shall not be liable for any loss, actions, claims, proceedings, demand or costs or damages whatsoever or howsoever caused arising directly or indirectly in connection with or arising out of the use of this material.

## RESEARCH ARTICLE

### Strong-field control of electron localisation during molecular dissociation

M.F. Kling<sup>ab\*</sup>, Ch. Siedschlag<sup>a</sup>, I. Znakovskaya<sup>b</sup>, A.J. Verhoef<sup>b</sup>, S. Zherebtsov<sup>b</sup>,  
F. Krausz<sup>bc</sup>, M. Lezius<sup>b</sup> and M.J.J. Vrakking<sup>a</sup>

<sup>a</sup>FOM Instituut voor Atoom en Molecuul Fysica (AMOLF), 1098 SJ Amsterdam, The Netherlands;

<sup>b</sup>Max-Planck-Institut für Quantenoptik, D-85748 Garching, Germany;

<sup>c</sup>Department für Physik, Ludwig-Maximilians-Universität München,  
D-85748 Garching, Germany

(Received 24 October 2007; final version received 10 December 2007)

We demonstrate how the waveform of light can be used to control a molecular dissociation by the steering and localisation of electrons. Experimental results have been obtained for the dissociative ionisation of the homonuclear and heteronuclear hydrogen derivatives D<sub>2</sub> and HD. Asymmetric ejection of the ionic fragments reveals that light-driven electronic motion prior to dissociation localises the electron on one of the two ions in diatomic molecular ions in a controlled way. Extension of these results to electron transfer in complex molecules suggests a new paradigm for controlling photochemistry.

**Keywords:** strong-field control; few-cycle laser pulses; charge localisation

#### 1. Introduction

Coherent control of molecular dynamics has entered a new and exciting regime with the advent of intense few-cycle phase-stabilised laser pulses [1]. Laser technology now allows for the generation and control of electromagnetic fields, where the electric field can be switched between 0 and several a.u. with a temporal accuracy of a few 100 as [2]. Obviously, only electrons can respond on this timescale, and atomic centers will remain frozen. If the laser intensity is chosen carefully, the extreme nonlinearity of the strong field tunneling probability due to the Gamov factor  $\exp(-2(2U_1)^{3/2}/3|E(t)|)$ , with  $U_1$  the ionisation potential and  $E(t)$  the electric field, leads to situations where electrons are liberated from a molecule within a fraction (100–300 as) of the cycle of the carrier wave. A full cycle of this carrier wave typically lasts about 2660 as at 800 nm when using Ti:sapphire lasers. Subsequently, these electrons are driven by the laser field [3], which leads to daughter processes that can, in principle, be precisely synchronised with respect to the original ionisation event. Typical cases are recombination and high-order harmonic generation [4], scattering and high-energy above-threshold ionisation (ATI) [5,6], as well as attosecond electron diffraction [7]. All of these processes take place about one-third of the laser cycle after strong field ionisation (SFI) has happened

close to the peak electric field [3], when the electron revisits its parent near a zero-crossing of the electric field. The electron rescattering process can also lead to population transfer into excited states above the ionic ground state, which is usually prepared during the strong field tunneling process. This is especially attractive to molecular physics, because the preparation of higher excited molecular states can thus be very precisely timed. Furthermore, because electron rescattering is approximately equal to classical electron impact excitation of ions, no strong selection rules apply, in contrast to the optical case. Only if during rescattering recombination takes place, will the molecule preferentially end up in its initial state, and excess energy will be given away as harmonic radiation. This has been used with advantage for the prominent tomographic imaging of molecular orbitals by Itatani *et al.* [8]

Molecular electron rescattering physics can, and has been, investigated intensively by various groups in recent years with multi-cycle laser pulses. However, for the case where the laser pulse duration approaches the optical period, one enters the few-cycle regime and the electromagnetic driver fields become increasingly asymmetric. Such fields have recently opened up new avenues for coherent control. Spatial control of electron emission has been observed and has become a major tool for

\*Corresponding author. Email: matthias.kling@mpq.mpg.de

long-term stabilisation of the laser phase [9]. It has also been possible to control total fragment particle momenta [10]. The prerequisite for such experiments, control of the carrier-envelope phase (CEP) itself, has become available as a laser control parameter since the ground-breaking work of Hänsch and coworkers [11], and its extension to amplified laser systems by Baltuska *et al.* [2]. The latter has paved the way into the strong field community. Stabilisation and control of the laser phase with comparably high precision has made many experiments possible that are directly related to attosecond physics [12–18]. The relation between the CEP and attosecond physics itself can be easily understood, since control over the CEP is virtually equal to control of a light field with attosecond precision. CEP control applied to the few-cycle regime, however, enables access to mono-cycle strong field ionisation. In such cases, subsequent steering of isolated attosecond electron wavepackets is feasible and gives access to controlled time-dependent and intense polarisation of the target system. In combination with molecular alignment or orientation selection via SFI the technique can be used to control the final localisation of charge during molecular dissociation, as has been previously demonstrated for the D–D homonuclear dimer [15]. In this paper, we extend the discussion of such experiments to the heteronuclear dimer H–D, and to additional aspects in the CEP control of charge redistribution, which may be attributed to phase control of bond-softening processes.

Hydrogen ionisation and dissociation has been attractive to the femtosecond community for several years (see, e.g., reference 19 and references therein). Some reasons for this are, firstly, H<sub>2</sub> intra-nuclear vibrational wavepacket dynamics is very fast and requires a temporal resolution in the few-fs regime [20]. Second, because only two electrons and two protons are involved, the system can be numerically accessed with high accuracy [21]. As such, it has model character for the treatment of more complex molecules and with regard to chemistry perhaps more interesting cases. Third, the lower ionic levels in hydrogen are energetically well separated [22,23]. Because of this, IR multiphoton ionisation ends up mostly in one single electronic state ( $1s\sigma_g^+$ ). Subsequent electron rescattering events then populate a superposition of higher states, e.g. create a synchronised electronic wavepacket. The corresponding coupled electron–nuclear dynamics evolving within the rapidly decaying strong laser field can be made responsible for final charge localisation [15,24–26].

## 2. Experimental

The experimental scheme used here has been described earlier [15]. In brief, transform-limited laser pulses of 25 fs duration with 1 mJ pulse energy were generated with a 3 kHz phase-stabilised amplified Ti:sapphire laser system (Femtolasers, Femtopower Compact Pro). The pulse was spectrally broadened using a 1 m long hollow-core fiber of 250  $\mu\text{m}$  diameter filled with 3.8 bar neon gas. The laser pointing into the fiber was controlled with high precision with a home-built stabiliser system consisting of a CCD camera and a motorised mirror mount. The output pulses from the fiber exhibited a significantly broadened spectrum [27] and were compressed down to a near-transform limited duration of  $\sim 5$  fs using eight reflections in a chirped mirror compressor. By tuning of the gas pressure in the hollow-core fiber the pulse length was adjusted precisely between 25 and 5 fs. The pulse duration was monitored online with a commercial dispersion balanced autocorrelator. The laser phase was stabilised with a feedback loop [28,29]. The polarisation is rectified using three 5  $\mu\text{m}$  thick pellicles at the Brewster angle. Fine tuning of the pulse duration and varying the CEP was done by changing the amount of material dispersion with a pair of fused-silica wedges after the hollow fibre. The phase jitter was smaller than 150 mrad. Phase-stabilised, linearly polarised pulses at a central wavelength of 760 nm were focused with a spherical mirror ( $R=80$  cm) into the center of the ion optics of a velocity-map imaging spectrometer (Figure 1(a)) [20]. In the focus intensities of up to  $5 \times 10^{14} \text{ W cm}^{-2}$  were realised, and an adjustable iris was used to vary the intensity in the focus. Ions and electrons were generated at the crossing point between the laser and the molecular beam (with a particle density of approximately  $10^{13} \text{ cm}^{-3}$ ) and were accelerated and focused with the ion optics onto a MCP phosphor screen assembly (Hamamatsu, F2226-24PX). The molecular beam was produced by a pulsed nozzle of 1 mm diameter and operated at 50 Hz. The molecular beam was differentially pumped and passed a skimmer of 1 mm diameter 10 cm downstream before entering the interaction region. The sensitivity of the MCP detector was switched so that only ions or electrons from every 60th laser pulse were detected. This allowed for a low background pressure in the chamber (typically  $2 \times 10^{-7}$  mbar). The velocity map images were recorded with a CCD camera (Pulnix, TM-9701) and were typically averaged over 60 s of data acquisition for each setting of the laser phase.

Figure 1(B) shows a typical experimental momentum map of D<sup>+</sup> ions recorded with 5 fs excitation at  $10^{14} \text{ W cm}^{-2}$  without CEP stabilisation. The laser

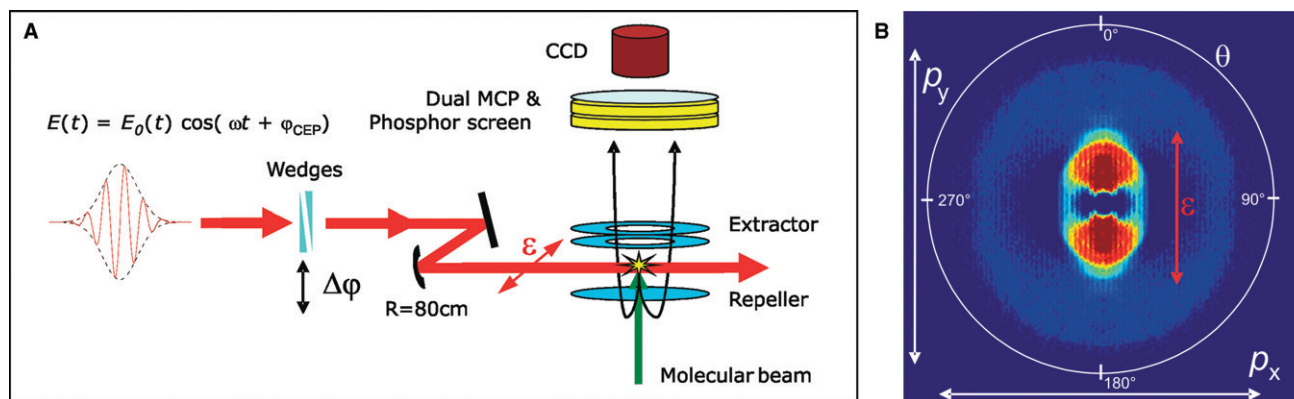


Figure 1. (a) Schematic view of the velocity map imaging experiment. Laser pulses are CEP controlled using a pair of wedges. The beam is focused with a spherical mirror ( $f=40$  cm) into the center of the ion optics, where it crosses a molecular beam. The resulting ions are extracted and analysed using a dual microchannel and phosphor screen detector. (b) A typical velocity map image from the detection of  $D^+$  ions in the dissociation of  $D_2$  with 5 fs pulses at  $10^{14} \text{ W cm}^{-2}$  without phase stabilisation.

was polarised along the  $p_y$  axis. Two main contributions are visible in both upwards and downwards emission direction: a strong peak at lower energies with a relatively narrow angular distribution and a contribution at larger momenta with a wide angular distribution. After inversion of the image using an iterative inversion procedure [31], the original 3D momentum distribution can be reconstructed. By integration of the inverted image over the full solid angle the energy spectrum displayed in Figure 2(A) is derived. The spectral features can be attributed to the following reaction pathways (as sketched in Figure 2(C)).

- (A) Following strong-field tunnel ionisation of  $D_2$  with the production of an electron and a  $D_2^+$  ion in the  $1s\sigma_g^+$  state, recollisional excitation (RCE) [32,33] to the  $2p\sigma_u^+$  state by the returning electron leads to dissociation and formation of  $D^+$  and  $D$  fragments with energies above 3 eV. This channel shows a broad angular distribution as seen in Figure 2(B), in agreement with earlier observations [34]. Note that no ions at these energies are observed with circular polarised light (Figure 2(A)), strongly supporting recollision to be responsible for their production.
- (B) Close to the outer turning point of the nuclear wavepacket, bond softening (BS) [19,35,36] becomes a prominent process, leading to very low fragment energies below 3 eV with its main contribution between 0 and 2 eV.
- (C) At the intensities used in these studies, Coulomb explosion of  $D_2$  with the production of two  $D^+$  ions is possible via enhanced

ionisation (EI). This channel is, however, unwanted for the present investigations and therefore we tried to keep such signals at a minimum. In fact, only a minor contribution of EI is seen between 2 and 3 eV, which exhibits a smaller angular distribution than the BS pathway (see Figure 2(B)).

### 3. Results I: electron localisation in $D_2$

In order to elucidate the role of the CEP in the experimental ion momentum distributions, the laser phase was scanned carefully over a range of multiple cycles. The angle-integrated asymmetry in the ion momentum distribution at a certain energy  $W=p^2/(2m)$  and phase  $\varphi$  was obtained from

$$A(W, \varphi) = \frac{P_{\text{up}}(W, \varphi) - P_{\text{down}}(W, \varphi)}{P_{\text{up}}(W, \varphi) + P_{\text{down}}(W, \varphi)}, \quad (1)$$

with

$$P_{\text{up}}(W, \varphi) = \int_{330}^{360} \int_0^{360} P(W, \theta, \phi, \varphi) d\phi \sin \theta d\theta + \int_0^{30} \int_0^{180} P(W, \theta, \phi, \varphi) d\phi \sin \theta d\theta, \quad (2)$$

and

$$P_{\text{down}}(W, \varphi) = \int_{150}^{210} \int_0^{360} P(W, \theta, \phi, \varphi) d\phi \sin \theta d\theta, \quad (3)$$

with  $\theta$  and  $\varphi$  being the polar and azimuthal angles, respectively. We chose to analyse ion emission within a

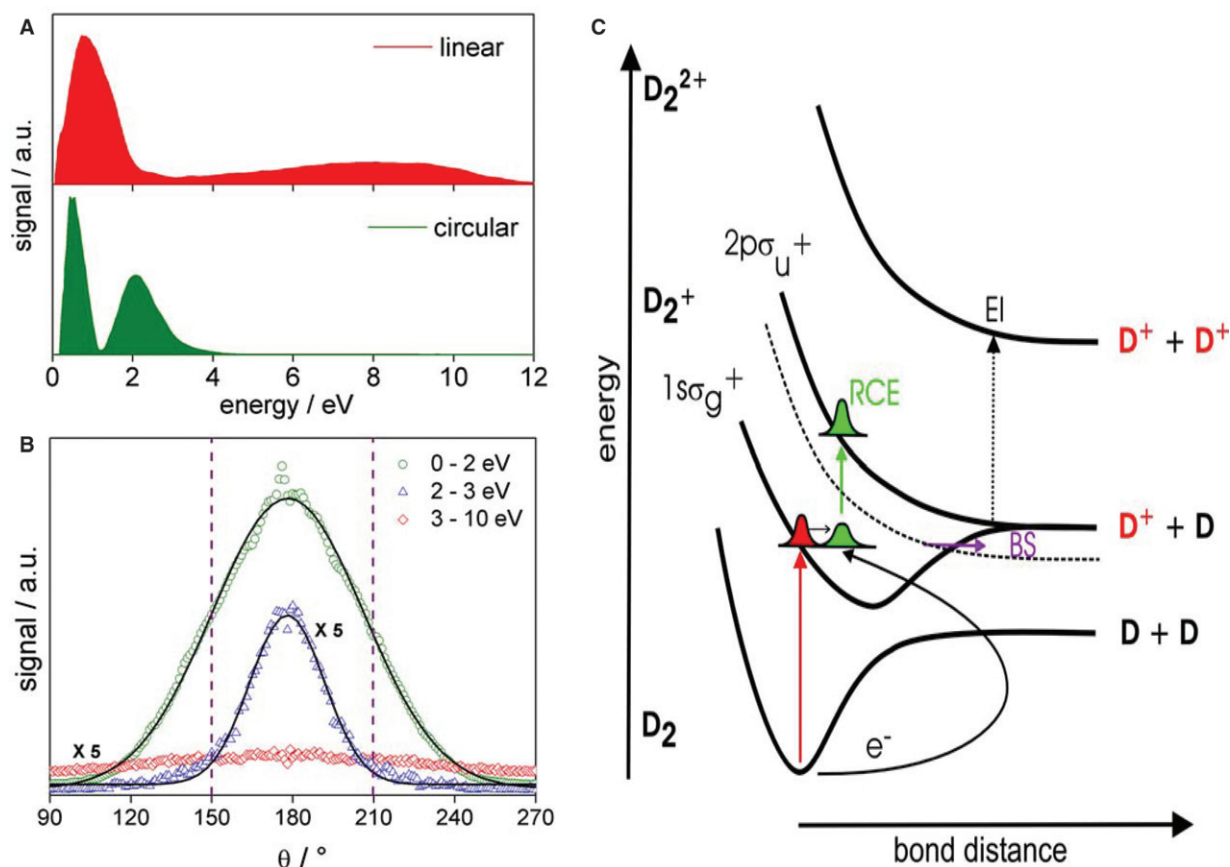


Figure 2. (A)  $D^+$  kinetic energy spectrum from the interaction of  $D_2$  with 5 fs linear and circular polarised laser pulses at  $10^{14} \text{ W cm}^{-2}$  without phase stabilization. (B) Angular distributions for  $D^+$  from  $D_2$  within three energy windows corresponding to the BS (0–2 eV), EI (2–3 eV) and RCE (3–8 eV) channels as measured for the conditions in (A) for linear polarization. (C) Schematic diagram showing the different dissociation pathways that yield  $D^+$  ions from  $D_2$  via dissociation of the molecular ion via recollisional excitation (RCE) or Coulomb explosion of  $D_2^+$  in enhanced ionisation (EI); in strong laser fields, bond softening (BS) may lead to dissociation of the molecular ion, where the avoided crossing between the diabatic potentials that are dressed by the laser field (as an example, the  $2p\sigma_u^+$  potential dressed with  $(-1)$  photon is drawn as a dashed line) results in an energy gap that gives rise to dissociation from vibrational levels that were originally bound [35]. BS has been studied in great detail for different light intensities and pulse durations [47]. Note that further channels playing a role at higher intensities than in the present studies are omitted from the scheme.

restricted angular range because our ability to control electron motion in hydrogen requires that the laser couples the two lowest-lying electronic states. For molecules aligned orthogonally to the laser polarisation axis, this coupling would be absent.

The contour plot in Figure 3(A) shows the measured angle-integrated asymmetry  $A(W, \varphi_{\text{CEP}})$  for dissociative ionisation of  $D_2$  into  $D^+ + D$  as a function of the carrier-envelope phase  $\varphi_{\text{CEP}}$  ( $x$  axis) and the kinetic energy  $W$  of the  $D^+$  ion fragment ( $y$  axis, see also Figure 2). Note that here the laser phase is only given as a relative number as the absolute phase has not been determined. Figure 3(A) shows that, in the energy range between 3 and 8 eV, locking of the laser phase in the few-cycle limit causes a remarkable asymmetry in the upward and downward emission. Regions in Figure 3(A) where the asymmetry oscillates

as a function of the phase represent the final energies of the  $D^+$  ions where the direction of their emission is effectively controlled by the sub-cycle evolution of the laser field driving the photodissociation. The extent of this ability to control is further illustrated in Figure 3(B), which displays asymmetries that are integrated over selected energy intervals. The highest degree of asymmetry, with a modulation depth of up to 45%, is observed between 3 and 8 eV. Above 8 eV, the asymmetry appears to cease completely. A very small phase dependence is seen between 1 and 2 eV (see also Figure 3(B)), which represents the typical energy range for bond softening. Most interestingly, this low-energy channel for charge localisation appears to be out of phase by ca.  $\pi/2$  with respect to the high-energy channel. In principle, when using 5 fs laser pulses, bond softening would not be expected, since this process

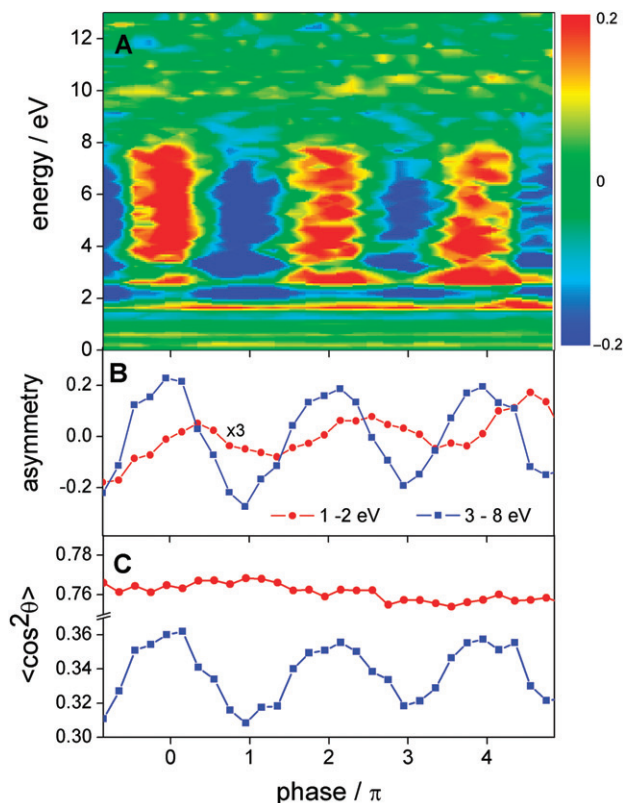


Figure 3. (A) Map of asymmetry parameter  $A(W, \theta)$  as a function of the  $\text{D}^+$  kinetic energy  $W$  and the carrier envelope phase  $\varphi_{\text{CEP}}$  (measured over a range of  $6\pi$  with a step size of  $0.1\pi$ ). (B) Asymmetry integrated over several energy ranges versus the CEP. (C) Degree of alignment of  $\text{D}^+$  ions (represented by the expectation value of  $\cos^2(\theta)$ ) versus the CEP for the same energy intervals as in (B).

requires motion of the vibrational wave packet that is formed by tunnel ionisation to the outer turning point of the  $1s\sigma_g^+$  potential well. This is expected to take about half a vibrational period, i.e. 12 fs in the case of  $\text{D}_2$  [37]. However, in our experiments the pulse contrast was not ideal. The background present in the few-cycle pulses amounted to ca. 10% in intensity at times when the internuclear distance moves into the BS region and might contribute to the asymmetry [26].

Plots of the expectation value of the alignment parameter  $\cos^2(\theta)$  versus the phase  $\varphi_{\text{CEP}}$  are given in Figure 3(C) and show the degree of alignment of  $\text{D}^+$  ions within the energy ranges used in Figure 3(B). A strong phase dependence is again seen for the energy range between 3 and 8 eV. This phase dependence is not present in the low-energy contribution. A comparison of Figures 3(B) and (C) indicates that the observation of a large asymmetry between 3 and 8 eV correlates with a greater degree of alignment.

The relation between the charge localisation process and the angular distribution of the fragment ions is further explored in Figure 4(A), where the amplitude  $A_0(W, \theta)$  of the asymmetry oscillation  $A((W, \theta, \varphi_{\text{CEP}}) = A_0(W, \theta) \sin((\varphi_{\text{CEP}} + \varphi_0 W, \theta))$  is shown as a function of kinetic energy  $W$  and fragment angle  $\theta$ . Clearly, for fragment angles  $\theta > 50^\circ$  the asymmetry vanishes. Moreover, a butterfly shape of the asymmetry amplitude is apparent and indicates different mechanisms for the generation of the asymmetry at low and high energies. This will be discussed in more detail below. Additionally, Figure 4(B) shows the asymmetry dependence on the pulse duration, which declines quasi-exponentially from ca. 45% close to 5 fs towards 1% above 9 fs. This behaviour reveals that the asymmetry of the field is driving the charge localisation process and that few-cycle pulses are an important prerequisite for the electron localisation control that has been achieved.

#### 4. Theoretical interpretation of the charge localisation effect in $\text{D}_2$

The electron localisation control in the fragmentation of  $\text{D}_2$  arises due to a phase control mechanism that consists of two parts. The first part has already been partially discussed in relation to the results shown in Figure 2(A). The absence of fragments in the kinetic energy range between 3 and 8 eV (where the observed asymmetry is most pronounced) in experiments using circularly polarised light strongly suggests the involvement of a re-collision of the electron that is ejected in the tunnel ionisation that produces the  $\text{D}_2^+$  ion. Our interpretation is that re-collision of this electron with the  $\text{D}_2^+$  ion leads to excitation of the  $\text{D}_2^+$  ion from the  $1s\sigma_g^+$  state to the dissociative  $2p\sigma_u^+$  state. Further, indirect support for this is provided by the observation of  $\text{D}^+$  fragments with a kinetic energy of up to 12 eV, consistent with acceleration along a repulsive curve starting from an internuclear distance close or equal to the internuclear distance in the neutral ground state. However, this re-collision excitation by itself is not enough to cause an asymmetry. If the observation of a high kinetic energy  $\text{D}^+$  fragment could be used as an indication of the fact that a fragment had been detected that was dissociating along the  $2p\sigma_u^+$  potential curve, then the molecule would retain its parity up to the point of detection, and – parity being a symmetry property of the electronic wave function – the distribution of the electron over the two  $\text{D}^+$  ions involved in the dissociation would necessarily have to be symmetric. A second ingredient is required, which breaks the parity of the electronic wave function.

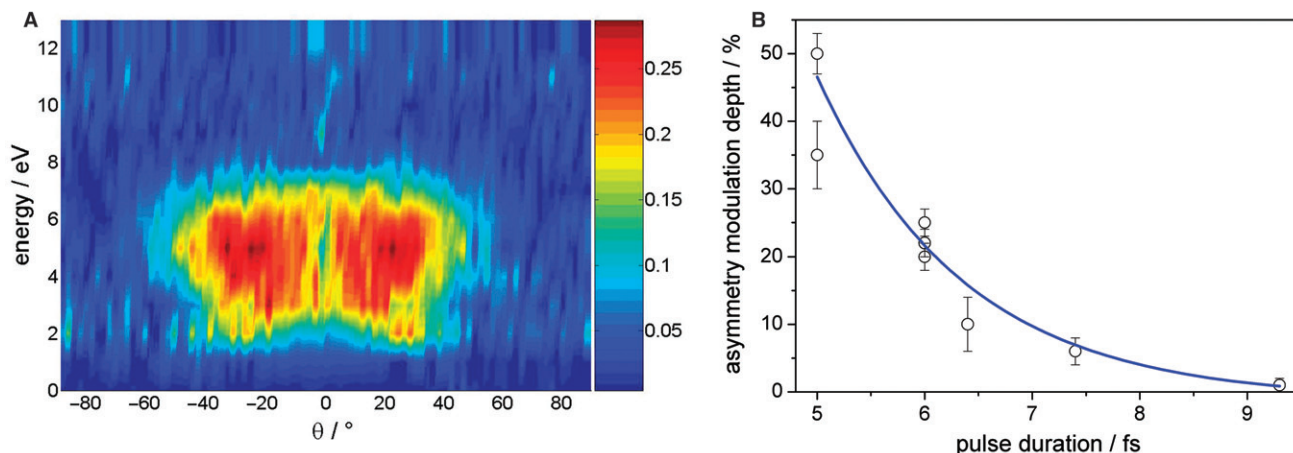


Figure 4. (A) Maximum degree of asymmetry  $A_0(W, \theta)$  in the emission of  $D^+$  ions from the dissociative ionization of  $D_2$  as a function of the emission angle and energy. The phase-dependent asymmetry oscillations have been fit to sine functions  $A(W, \theta, \varphi_{\text{CEP}}) = A_0(W, \theta) \sin(\varphi_{\text{CEP}} + \varphi_0(W, \theta))$  to obtain the parameter  $A_0(W, \theta)$ . The effect is limited to  $\theta = \pm 50^\circ$ . The butterfly shape of the effect indicates two different mechanisms, based on RCE for high energies and BS for small ion energies (see text). (B) Experimental dependence of the asymmetry modulation depth in the emission of  $D^+$  ions between 3 and 8 eV from dissociation of  $D_2$  on the laser pulse duration.

As has been proposed [15], and subsequently confirmed in more detailed theoretical treatments [21,25], laser-induced coupling between the  $2p\sigma_u^+$  and the  $1s\sigma_g^+$  states can convert the dissociative wave packet that starts out on the  $2p\sigma_u^+$  state into a coherent superposition state containing contributions from both the  $2p\sigma_u^+$  state and the  $1s\sigma_g^+$  state and – importantly – with a broken parity.

According to the presented simplified semiclassical model [15] the time evolution of the wave function for the hydrogen molecule after recollision can be calculated by expanding the full wave function for the electronic coordinate and the internuclear distance in terms of the lowest-lying electronic states,

$$\Psi(\mathbf{r}, R; t) \approx |g\rangle\psi_g(R; t) + |u\rangle\psi_u(R; t), \quad (4)$$

where  $|g\rangle$  and  $|u\rangle$  correspond to the  $1s\sigma_g^+$  and  $2p\sigma_u^+$  states, respectively, and where  $\psi_{g/u}$  represent the corresponding nuclear wave packets. In accordance with our observation that the asymmetry is primarily detected for fragments that are ejected along the laser polarisation axis, the molecule is assumed to be aligned along the axis of the laser field. Further support for this assumption comes from the fact that aligned molecules are preferentially ionised via SFI. By inserting this Ansatz into the time-dependent Schrödinger equation, one obtains the coupled equations:

$$i\frac{\partial}{\partial t} \begin{pmatrix} \psi_g(R; t) \\ \psi_u(R; t) \end{pmatrix} = \begin{pmatrix} -\frac{1}{M} \frac{\partial^2}{\partial R^2} + V_g(R) & V_{gu}(R) \\ V_{gu}^*(R) & -\frac{1}{M} \frac{\partial^2}{\partial R^2} + V_u(R) \end{pmatrix} \begin{pmatrix} \psi_g(R; t) \\ \psi_u(R; t) \end{pmatrix}, \quad (5)$$

with the binding potential curve  $V_g(R)$ , the dissociative curve  $V_u(R)$  and the coupling between them  $V_{gu}(R)$ . Tabulated values for the potential curves were used [22]. Integration of Equation (5) yields the time-dependent nuclear wave functions. The initial condition directly after the recollision consists of placing the vibrational ground state, obtained by relaxation on the respective potential curve [23], onto the dissociative potential curve of the molecular ion ( $2p\sigma_u^+$ ). The recollision time for the first recollision is 1.7 fs after ionisation [32]. Due to the fact that the experiment employed few-cycle pulses, later recollision events are considered to be efficiently suppressed [21,34]. We note that the ionisation is considered as a single event that occurs at the maximum of the laser electric field. This is a simplification, since the application of ADK theory [38] would predict that the ionisation may occur during more than a single half-cycle of the laser, and, furthermore, during a finite time interval within each half-cycle. A very rigorous theoretical treatment of the dynamics that goes well beyond the approach here and includes the ionisation and recollision steps was recently presented by Gräfe and Ivanov [25]. However, a computational treatment of hydrogen dissociation starting with an ADK treatment of the ionisation is beyond the scope of the present paper, where our main aim is to qualitatively explain the physics responsible for the observed phase control.

In the approach used here, for the calculation of the asymmetry, the electronic basis is changed to two states that are localised on the left and on the right

nucleus, respectively. Without loss of generality, we define

$$|l\rangle = \frac{1}{\sqrt{2}}(|g\rangle + |u\rangle), \quad (6)$$

and

$$|r\rangle = \frac{1}{\sqrt{2}}(|g\rangle - |u\rangle). \quad (7)$$

By projecting onto these states, the corresponding nuclear wave functions are obtained:

$$\psi_l(R; t) = \frac{1}{\sqrt{2}}(\psi_g(R; t) + \psi_u(R; t)), \quad (8)$$

$$\psi_r(R; t) = \frac{1}{\sqrt{2}}(\psi_g(R; t) - \psi_u(R; t)). \quad (9)$$

From these expressions the ( $t$ - as well as  $R$ -dependent) probabilities for the electron remaining on the left or on the right atom are calculated:

$$P_l(R, t) = \frac{1}{2} |\psi_g(R; t) + \psi_u(R; t)|^2, \quad (10)$$

$$P_r(R, t) = \frac{1}{2} |\psi_g(R; t) - \psi_u(R; t)|^2. \quad (11)$$

The time-dependent electron localisation parameter is then defined as

$$\frac{\int (P_l(R, t) - P_r(R, t)) dR}{\int (P_l(R, t) + P_r(R, t)) dR}. \quad (12)$$

From these expressions we can immediately see that it is the coherent superposition of the two electronic states  $1s\sigma_g^+$  and  $2p\sigma_u^+$  that is responsible for the asymmetry in the charge localisation.

Figure 5 displays the temporal evolution of the laser field and the time-dependent electron localisation parameter quantifying the localisation on the upper/lower nucleus. The initial asymmetry that develops in the electron density is synchronised to the laser frequency, the intuitive picture being that the laser drives the electron back-and-forth (on attosecond timescales) between the two nuclei. However, as the molecule dissociates, the oscillatory motion of the electron between the two nuclei is impeded by the emergence of a potential barrier between the two nuclei. For an internuclear distance that is close to the internuclear distance where enhanced ionisation would occur, the electron oscillation stops and the electron density is found to localise predominantly on one of the atoms. In agreement with the experimental observation, shifting the CEP by  $\pi$  turns the laser field and thus the asymmetry around.

The observation of asymmetric  $D^+$  emission as a result of electron localisation requires that, in our

velocity-resolved  $D^+$  measurements, we are unable to identify the quantum path (i.e. the  $1s\sigma_g^+$  or the  $2p\sigma_u^+$  curve) along which the measured ions were created. This restricts the kinetic energy range where an asymmetric emission may be expected. In good agreement with experiment, the asymmetry is calculated to peak at around 6 eV. Importantly, no electron localisation is observed at the very highest kinetic energies that occur in the experiment, since the wave packet that dissociates on the  $1s\sigma_g^+$  curve is necessarily slower than the wave packet that dissociates on the repulsive  $2p\sigma_u^+$  curve. In the intermediate energy range between 2 and 8 eV the charge localisation phase dependence exhibits, if at all, only weak substructures. This behaviour may originate from the electron rescattering process, which allows for access to a broad energetic range in molecular excitation during the sub-cycle rescattering event. The interpretation of the low KER regime is, however, more complicated. Simulations [21] show a larger phase offset of  $\sim\pi$  between BS and RCE. As suggested by Roudnev and Esry [39], asymmetries could be the result of pure interference between the  $1s\sigma_g^+$  and  $2p\sigma_u^+$  molecular channels populated directly via sequential optical excitation. If the nuclei are dissociating in two different molecular channels, they can still contribute at the same kinetic energy. In the few-cycle case, laser bandwidth and Stark-shifting of the initial state may be strong enough to create this overlap of nuclear wavepackets, so that the relative phase between the final components still depends on the CEP.

Another, quite interesting aspect comes into play from the  $\theta$  dependence of the asymmetry as illustrated in Figures 3(C) and 4(A). Within our simplified model, interference at low dissociation energies means that the low-energy tail of the dissociative excited state wavepacket is interfering with a wavepacket that must have been stimulated from  $2p\sigma_u^+$  to  $1s\sigma_g^+$  by the laser field relatively early after the rescattering excitation process. We suggest that early de-excitation should be more dependent on the molecular alignment, which would explain why, in Figure 4, the low-energy region populates a smaller angular range. On the other hand, interference at high energy means that the downward transition takes place relatively late. When the gap between the two potential curves becomes less than a photon, it should suddenly become very difficult to induce a transition and only the very well aligned molecules may still succeed. Again, the angular selection becomes stricter, as observed in our experiment.

To conclude, within our modeling, we understand final charge localisation during molecular dissociation in the following way. The molecular ions are formed in a (single) ionisation event that occurs at the

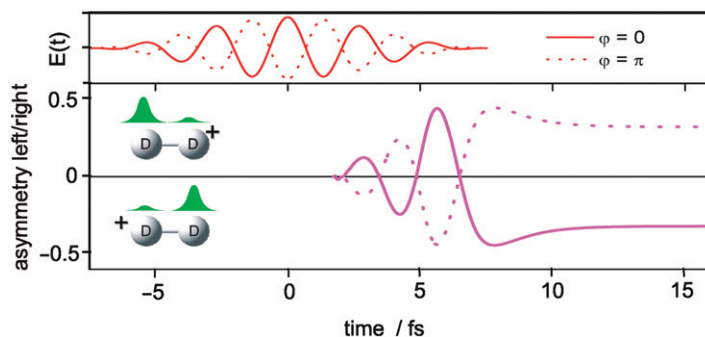


Figure 5. Results of the simulations: about two-thirds of an optical cycle after an electron has been liberated from the neutral molecule (accompanied by the production of a wave packet evolving along the ground ionic state  $1s\sigma_g^+$ ), this electron recollides with the parent and excites the part of the population that is relevant for the explanation of the experimental results for the  $2p\sigma_u^+$  state. Superposition of both the  $1s\sigma_g^+$  and  $2p\sigma_u^+$  states is formed in the laser field by population transfer. This breaks the parity of the electronic wavefunction, and allows control of the final localisation of the charge on the ‘left’ and the ‘right’ part of the molecule.

maximum of the laser electric field. The ionisation event starts a vibrational wave packet in the  $1s\sigma_g^+$  ground electronic state of  $D_2^+$  that mimics the vibrational ground-state wave function of  $D_2$  before excitation. Rescattering then leads to population transfer from the  $1s\sigma_g^+$  ground electronic state to the  $2p\sigma_u^+$  excited electronic state at a delay of  $\sim 1.7$  fs after ionisation [32]. Because of the strongly repulsive nature of the  $2p\sigma_u^+$  state, the excited  $D_2^+$  molecule rapidly dissociates and the resulting fragments acquire significant kinetic energies up to 10 eV. During molecular dissociation the laser field can, however, transfer part of the  $2p\sigma_u^+$  population back into the  $1s\sigma_g^+$  state, thereby producing a dissociative wave packet with large excess kinetic energy. The emerging coherent superposition of the two electronic states results in a time-dependent localisation of the electron density on the upper or lower nucleus due to the gerade and ungerade nature of the two states.

## 5. Results II: electron localisation in HD

Following the experimental demonstration of CEP control of electron localisation in  $D_2$ , further experiments were performed exploring the possibility of controlling electron localisation in HD. Figure 6(A) shows the  $D^+$  ion kinetic energy spectrum that is obtained after excitation of HD with 5 fs laser pulses at  $10^{14} \text{ W cm}^{-2}$ . Unlike the case of  $D_2$ , the HD measurements were successfully accompanied by a measurement of above-threshold ionisation in Xe, allowing us to assign a CEP of  $\pi/5$ . The insert depicts a typical velocity map image, from which the energy spectrum was obtained after angular integration. By varying the CEP an asymmetry map  $A(W, \varphi_{\text{CEP}})$  was obtained (see Figure 6(B)). In comparison with the homonuclear

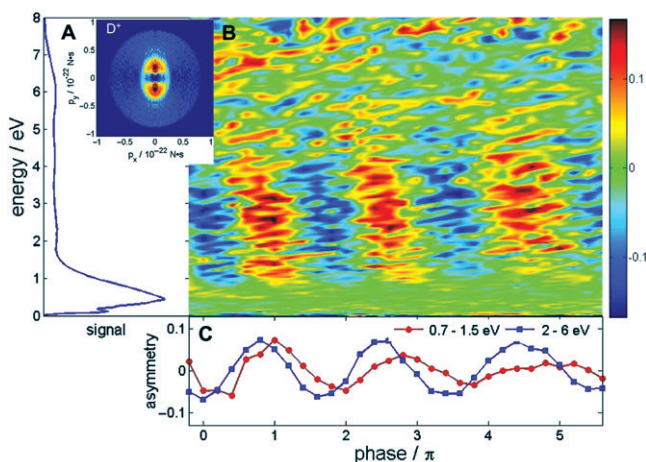


Figure 6. Asymmetry data obtained for the case of HD,  $D^+$  ions. (A) Sample image and kinetic energy spectrum for  $D^+$  ions from the dissociation of HD with 5 fs,  $10^{14} \text{ W cm}^{-2}$  pulses. (B) Map of the asymmetry parameter  $A(W, \theta)$  as a function of the  $D^+$  kinetic energy  $W$  and phase  $\varphi_{\text{CEP}}$ . (C) Asymmetry parameter integrated over selected energy ranges (as indicated) versus the CEP.

$D_2$  case, quite similar asymmetries are obtained for the heteronuclear molecule. Figure 7(A) shows related data for  $H^+$  from HD for the same excitation conditions (5 fs,  $10^{14} \text{ W cm}^{-2}$ ). Note that the energy spectra differ by approximately a factor of  $\sqrt{2}$  due to momentum conservation during the dissociation process. In general, proton spectra tend to show more noise, because of an increased background from ionisation of  $H_2O$ . Apart from this additional noise, the  $D^+$  and  $H^+$  ion spectra shown in Figures 6 and 7 show very comparable asymmetry features. The asymmetries are also very similar to the homonuclear case displayed in Figure 3. As seen in Figure 6(B), for  $D^+$  the asymmetry becomes prominent

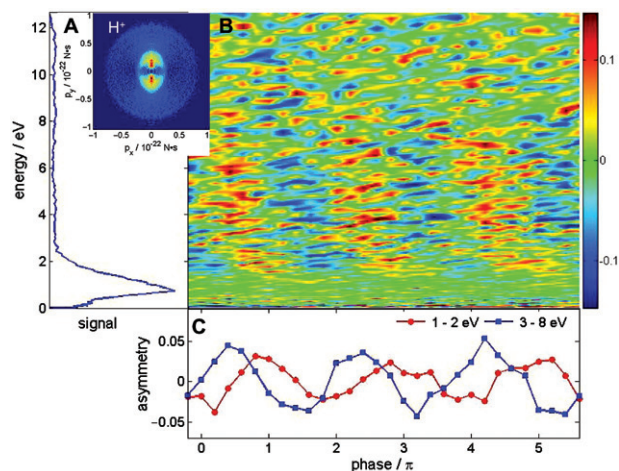


Figure 7. Asymmetry data obtained for the case of HD,  $\text{H}^+$  ions. (A) Sample image and kinetic energy spectrum for  $\text{H}^+$  ions from the dissociation of HD with 5 fs,  $10^{14} \text{ W cm}^{-2}$  pulses. (B) Map of the asymmetry parameter  $A(W, \theta)$  as a function of the  $\text{H}^+$  kinetic energy  $W$  and phase  $\varphi_{\text{CEP}}$ . (C) Asymmetry parameter integrated over selected energy ranges versus the CEP.

from 2 to 6 eV and for  $\text{H}^+$ , shown in Figure 7(B), between 3 and 8 eV. Note that the phase features of  $\text{H}^+$  and  $\text{D}^+$  in Figures 6 and 7 do not coincide fully, which is possibly due to the low signal-to-noise ratio in the  $\text{H}^+$  measurements. As for  $\text{D}_2$ , an asymmetry oscillation is also observed for HD at lower ion kinetic energies within the range of the bond softening contribution (0.7–1.5 and 1–2 eV for  $\text{D}^+$  and  $\text{H}^+$ , respectively). Again, a shift of the phase of the asymmetry oscillation between the low- and high-energy channels of approximately  $\pi/2$  is seen (see Figures 6(C) and 7(C)).

Figure 8 shows the energy and angular dependence of the amplitude  $A_0(W, \theta)$  of the asymmetry oscillation  $A(W, \theta, \varphi_{\text{CEP}}) = A_0(W, \theta) \sin(\varphi_{\text{CEP}} + \varphi_0(W, \theta))$  that was obtained for  $\text{D}^+$  ions from the dissociative ionisation of HD. Similar to Figure 4(A), where this analysis was performed for  $\text{D}_2$ , the asymmetry is restricted to angles  $\theta < 50^\circ$  and shows a significant difference in the angular distribution of the asymmetry between the low- (0.7–1.5 eV) and high-energy (above 2 eV) channels. The kinetic energy range where the asymmetries are observed for  $\text{H}^+$  and  $\text{D}^+$  from HD is lower than the kinetic range where these effects were observed for  $\text{D}_2$ . A possible reason for this may be the fact that the vibrational period of HD is shorter than that of  $\text{D}_2$ , meaning that the vibrational wave packet that is initially produced in the  $1s\sigma_g$  ground electronic state moves farther out during the 1.7 fs separating the ionisation and the recollision event. If so, recollision excitation promotes the nuclear wave packet to a somewhat lower position on the repulsive  $2p\sigma_u$  curve.

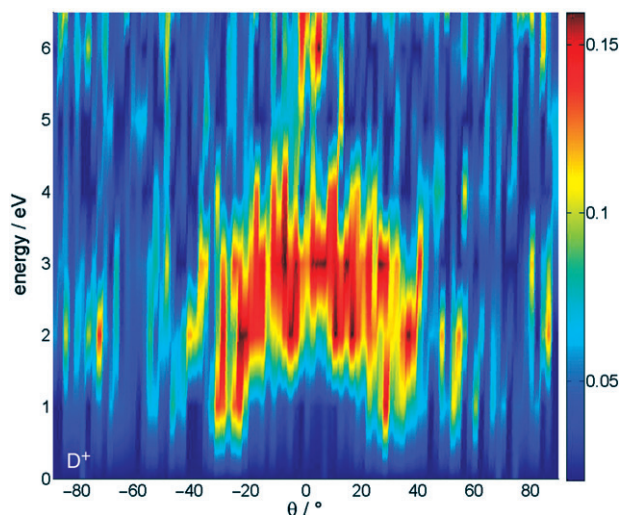


Figure 8. Maximum degree of asymmetry  $A_0(W, \theta)$  in the emission of  $\text{D}^+$  ions from the dissociative ionisation of HD as a function of the emission angle and energy. The phase-dependent asymmetry oscillations have been fit to sine functions  $A(W, \theta, \varphi_{\text{CEP}}) = A_0(W, \theta) \sin(\varphi_{\text{CEP}} + \varphi_0(W, \theta))$  to obtain the parameter  $A_0(W, \theta)$ .

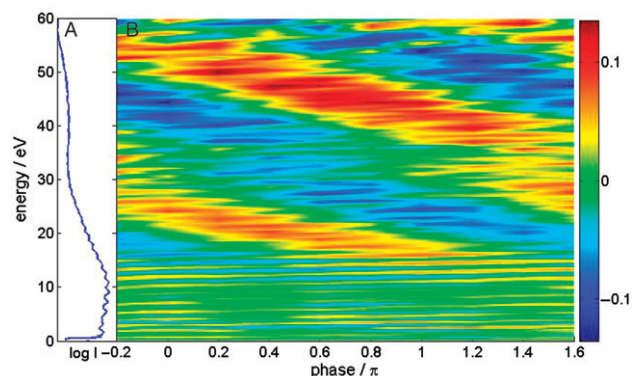


Figure 9. (A) Spectrum and (B) asymmetry map  $A(W, \varphi_{\text{CEP}})$  for the emission of electrons in the above-threshold ionisation of Xe with 5 fs pulses at  $10^{14} \text{ W cm}^{-2}$ . The phase was set to zero at the maximum asymmetry for cut-off electrons and used to calibrate the phase axis in Figures 6 and 7.

The CEP in Figures 6 and 7 was determined *in situ* as an absolute phase via a reference measurement of the asymmetry  $A(W, \varphi_{\text{CEP}})$  in the electron emission in the above-threshold ionization (ATI) of Xe (see Figure 9(A) for the ATI spectrum and 9(B) for the asymmetry map). The CEP was set to zero at positions where the cut-off electron emission reaches its maximum in the upward direction [40]. This should facilitate direct comparison with theoretical studies of the system. Interestingly, in HD, in agreement with recent theoretical findings [21], the emission of ions to one of the two sides of the laser polarisation does not

necessarily coincide with phase values of  $\varphi_{\text{CEP}} = n\pi$  (with integer number  $n$ ).

The phase difference between the high-energy (recollision) and low-energy (bond softening) channels in both  $\text{D}_2$  and HD of  $\sim\pi/2$  is reminiscent of shifts that have been reported between direct and rescattered ATI photoelectron spectra for rare gas atoms, which, for direct (low-energy) electrons, have been explained as a manifestation of double slits in time [14]. In the present experiment, however, the mechanism is slightly different. Based on inspection of the kinetic energy distributions in Figures 6 and 7 we have attributed the asymmetries at low energies to the onset of contributions from a (direct) bond softening (BS) channel, while higher energies have been attributed to (indirect) recollisional excitation (RCE). The difference in the ionisation mechanism is therefore, in principle, similar to that presented in reference 14. However, in the molecular case the closely coupled electron–nuclear dynamics has to be additionally taken into account. Thus, the asymmetry of the BS channel should rather be understood in terms of an  $n$ -photon pathway interference between the two respective trajectories for the dissociation of the hydrogen molecular ion. During evolution of the molecule the laser field can couple the gerade and the ungerade states directly when the wavepacket approaches the outer potential well [26]. This coupling may be responsible for the observed phase dependence as calculated by Roudnev and Esry for  $\text{HD}^+$  [39]. Moreover, weak phase shifted asymmetries for total ion kinetic energies below 5 eV have been observed [21] in  $\text{D}_2$  model calculations, and have been attributed to asymmetric dissociation [24].

## 6. Conclusion

Electron-transfer processes play a pivotal role in chemistry. Presently, following the generation and measurement of a single sub-femtosecond pulse made possible by unprecedented control of bound and free atomic electrons, respectively, with the sub-cycle evolution of a strong light field [41], it may be possible to observe electron-transfer processes on the fastest timescales that these processes take place. When attosecond pulses are used to initiate electron dynamics in molecules, the high photon energy of the attosecond pulse generally results in ionisation. As discussed by Remacle and Levine [42], removal of an electron on attosecond timescales will often result in the formation of electronic wave packets, because the electron–hole density that results from removing an electron from the highest-occupied molecular orbital (HOMO) does not match the electron–hole density in the singly occupied

HOMO of the cation formed on ionisation. Ultrafast removal of an electron therefore not only forms the ground electronic state of the cation, but, rather, a coherent superposition of electronic states. Remacle and Levine [42] have argued that the formation of this wave packet may lead to electron transport across the ionic structure that is formed. For example, the photoionisation of the neutral tetrapeptide molecule TrpLeu<sub>3</sub> is expected to lead to population of the HOMO-1 and the HOMO of the TrpLeu<sub>3</sub><sup>+</sup> cation. The shape of these orbitals and the 3 eV energy splitting between the two orbitals suggest that electron transfer from one end of the molecule to the other occurs in less than 1 fs. Comparing a wide range of electronic systems, Breidbach and Cederbaum [43] observed that the sudden removal of an electron is accompanied by a characteristic time response completed in approximately 50 as. This time response is interpreted in terms of a filling – upon ionisation – of the exchange-correlation hole associated with the electron ionised by its neighbouring electrons.

The time that sub-femtosecond pulses are used to initiate the formation and subsequently probe of an electron wavepacket that transfers electron density across a large molecule has not yet come. However, in the present paper we have extended sub-femtosecond electron control to molecules and obtained the first evidence of its usefulness in controlling reaction dynamics. We have controlled the dissociation of  $\text{D}_2^+$  and  $\text{HD}^+$  by steering electron wave packet motion with the sub-cycle, i.e. sub-femtosecond evolution of the electric field of a few-cycle light wave. A coherent superposition of two electronic states in the molecular ion is responsible for an oscillating electron density and the final localisation of the electron. While the computed electron and nuclear dynamics are consistent with our measurement, deeper insight into the role of field-controlled electron dynamics in driving chemical reactions will require time-resolved investigations [25,44,45]. The door to such studies is now open thanks to the availability of sub-femtosecond extreme-ultraviolet (XUV) pulses synchronised with the few-cycle control pulse [41]. Synthesised ultrawide-band (multi-colour) waveforms (comprising near-infrared, visible and possibly ultraviolet light), which can now both be produced and measured, may dramatically enhance the efficiency of steering reactions by creating electronic wave packets and subsequently driving them towards selected sites in complex molecular systems. Indeed, recent theoretical work suggests that circular electronic motion in ring-shaped molecules can be induced by controlled light-fields [46].

Electron-transfer processes are extremely important in chemistry and biology. For example, rapid electron transfer can promote both damage and repair of DNA base-pairs. Our results for the intense-field dissociative ionisation of D<sub>2</sub> and HD constitute a first example of the control of intra-molecular electronic dynamics under the influence of a laser phase and thus provide a first clue that intra-molecular electron transfer processes may be controllable by light fields of controlled evolution.

### Acknowledgements

We acknowledge contributions by Y. Ni, J.I. Khan, M. Schultze, T. Uphues, J. Rauschenberger, M. Uiberacker and M. Drescher to these studies. We thank the European Union for support by the Marie Curie Research Training Network XTRA, MRTN-CT-2003-505138, a Marie Curie Intra-European Fellowship, MEIF-CT-2003-500947, and a European Reintegration Grant. The research of M.F.K., C.S. and M.J.J.V. is part of the research program of the 'Stichting voor Fundamenteel Onderzoek der Materie (FOM)', which was financially supported by the 'Nederlandse Organisatie voor Wetenschappelijk Onderzoek (NWO)'. M.F.K., I.Z. and S.Z. acknowledge support by the Max-Planck Society and by the German Science Foundation via the Emmy-Noether program. This work was partly supported by the Cluster of Excellence 'Munich Center for Advanced Photonics' (MAP).

### References

- [1] M. Lenzner, *et al.*, IEICE Trans. **E81-C** (2), 112 (1998).
- [2] A. Baltuska, *et al.*, Nature. **421** (6923), 611 (2003).
- [3] M. Lewenstein, *et al.*, Phys. Rev. A **49** (3), 2117 (1994).
- [4] X.F. Li, *et al.*, Phys. Rev. A. **39** (11), 5751 (1989).
- [5] R.R. Freeman, *et al.*, Phys. Rev. Lett. **59** (10), 1092 (1987).
- [6] G.G. Paulus, *et al.*, Phys. Rev. Lett. **72** (18), 2851 (1994).
- [7] M. Spanner, *et al.*, J. Phys. B. **37** (12), L243 (2004).
- [8] J. Itatani, *et al.*, Nature. **432** (7019), 867 (2004).
- [9] G.G. Paulus, *et al.*, Phys. Rev. Lett. **91** (25), 253004 (2003).
- [10] X. Liu, *et al.*, Phys. Rev. Lett. **93** (26), 263001 (2004).
- [11] J. Reichert, *et al.*, Opt. Comm. **172** (1–6), 59 (1999).
- [12] E. Goulielmakis, *et al.*, Science. **305**, 1267 (2004).
- [13] R. Kienberger, *et al.*, Nature. **427** (6977), 817 (2004).
- [14] F. Lindner, *et al.*, Phys. Rev. Lett. **95** (4), 040401 (2005).
- [15] M.F. Kling, *et al.*, Science. **312** (5771), 246 (2006).
- [16] G. Sansone, *et al.*, Science. **314** (5798), 443 (2006).
- [17] M. Uiberacker, *et al.*, Nature. **446** (7136), 627 (2007).
- [18] A.L. Cavalieri, *et al.*, Nature. **449**, 1029 (2007).
- [19] J.H. Posthumus, Rep. Prog. Phys. **67** (5), 623 (2004).
- [20] A.S. Alnaser, *et al.*, Phys. Rev. A. **72** (3), 030702 (2005).
- [21] X.M. Tong and C.D. Lin, Phys. Rev. Lett. **98**, 123002 (2007).
- [22] J.M. Peek, J. Chem. Phys. **43** (9), 3004 (1965).
- [23] W. Kolos, K. Szalewicz, and H.J. Monkhorst, J. Chem. Phys. **84** (6), 3278 (1986).
- [24] A.D. Bandrauk, S. Chelkowski, and H.S. Nguyen, Int. J. Quant. Chem. **100** (6), 834 (2004).
- [25] S. Gräfe and M. Ivanov, Phys. Rev. Lett. **99**, 163603 (2007).
- [26] P. Haljan, M.Y. Ivanov, and P.B. Corkum, Laser Phys. **7** (3), 839 (1997).
- [27] A.L. Cavalieri, *et al.*, New J. Phys. **9** (7), 242 (2007).
- [28] J. Rauschenberger, *et al.*, Laser Phys. Lett. **3** (1), 37 (2006).
- [29] A.J. Verhoef, *et al.*, Opt. Lett. **31** (23), 3520 (2006).
- [30] F. Lepine, *et al.*, Phys. Rev. A **70**, 033417 (2004).
- [31] M.J.J. Vrakking, Rev. Sci. Instr. **72** (11), 4084 (2001).
- [32] H. Niikura, *et al.*, Nature. **417** (6892), 917 (2002).
- [33] H. Niikura, *et al.*, Nature. **421** (6925), 826 (2003).
- [34] A.S. Alnaser, *et al.*, Phys. Rev. Lett. **93** (18), 183202 (2004).
- [35] P.H. Bucksbaum, *et al.*, Phys. Rev. Lett. **64** (16), 1883 (1990).
- [36] H. Niikura, P.B. Corkum, and D.M. Villeneuve, Phys. Rev. Lett. **90** (20), 203601 (2003).
- [37] T. Ergler, *et al.*, Phys. Rev. Lett. **97** (19), 193001 (2006).
- [38] M.V. Ammosov, N.B. Delone, and V.P. Krainov, Sov. Phys. JETP. **64**, 1191 (1986).
- [39] V. Roudnev and B.D. Esry, Phys. Rev. A. **76**, 023403 (2007).
- [40] M.F. Kling, *et al.*, New J. Phys., submitted (2007).
- [41] E. Goulielmakis, *et al.*, Science. **317** (5839), 769 (2007).
- [42] F. Remacle and R.D. Levine, Proc. Natn Acad. Sci. U.S.A. **103** (18), 6793 (2006).
- [43] J. Breidbach and L.S. Cederbaum, Phys. Rev. Lett. **94**, 033901 (2005).
- [44] H. Niikura, *et al.*, J. Mod. Opt. **52** (2/3), 453 (2005).
- [45] G.L. Yudin, *et al.*, Phys. Rev. A. **72** (5), 051401 (2005).
- [46] I. Barth and J. Manz, Angew. Chem. Int. Ed. **45**, 2962 (2006).
- [47] K. Sändig, H. Figger, and T.W. Hänsch, Phys. Rev. Lett. **85** (23), 4876 (2000).